JOURNAL OF MATERIALS SCIENCE **36** (2001) 4027–4035

Carbon fibre-reinforced CMCs by PCS infiltration

H. Q. LY, R. TAYLOR, R. J. DAY
Manchester Materials Science Centre, University of Manchester/UMIST, Manchester, M1 7HS, UK
E-mail: richard.day@umist.ac.uk

C/SiC-based composites were produced by infiltration of a woven carbon fabric preform with a polycarbosilane (PCS) solution. Progress of the infiltration process up to eight infiltrations was followed by density measurements, microscopy and mechanical testing. After six infiltration cycles, the density increase tended to a plateau. Dense deposition of the matrix on the outer surface sealed off the core of the composite, which hindered successive infiltrations. With further re-infiltration cycles, the development of the matrix and the degree of bonding between the fibre and matrix increased. There was also a transition in the failure mode of the composite, when tested in 3-point bending, from shear to plain brittle tensile failure, as the number of infiltrations increased.

1. Introduction

Carbon-Carbon composites can have excellent specific strength up to high temperatures but the main drawback is their poor oxidation resistance. This may be overcome by replacing the carbon matrix with a refractory material such as SiC. Fibre-reinforced ceramic matrix composites (CMCs) have been prepared by various techniques [1]. Melt infiltration has, however, been limited to relatively low-melting glasses or glass ceramic systems. Conventional ceramic powder slurry methods which use high sintering temperatures and a pressing operation which can mechanically, thermally or chemically damage the fibres may cause severe reactions between the fibre and matrix [2, 3]. To overcome these problems, other infiltration routes, such as chemical vapour infiltration (CVI) and liquid silicon infiltration, have been used to form a SiC matrix in CMCs [4, 5]. These processes are, however, time consuming in the case of CVI due to the low deposition rates and can be deleterious in the liquid silicon route where the molten silicon will attack any exposed carbon fibres. A potential fabrication route is precursor polymer infiltration and pyrolysis. This is similar in principle to the formation of the carbon matrix in the preparation of C–C composites [6]. The SiC matrix is formed by the pyrolysis of an organosilicon polymer at around 1000 °C. Due to the high shrinkage and low SiC yield several re-infiltration steps are necessary [7–9]. Nevertheless, this process has the potential of having the advantage of a low processing temperature as in the CVI technique coupled with the ability to infiltrate large complex structures as in the liquid infiltration process. This is of particular interest in processing of 3-dimensional continuous fibre-reinforced composites, since these composites cannot be fabricated by pressure processes such as hot-pressing [10]. The PCS can be infiltrated into a preform as solution in a solvent [11] or a melt [12, 13] under vacuum. Filament winding with the fibres passing through the polymer solution has also been used [14, 15]. In this study, the progress of PCS solution infiltration of woven carbon fabric, after various cycles, was examined. This was evaluated by taking density/porosity measurements, microscopy and mechanical tests.

2. Experimental

2.1. Manufacture of composites

A 0/90° woven carbon fibre ((T300, manufactured by Toray) fabric, (supplied by Fothergill Engineered Fabrics)) was used. The preceramic polymer was a Polycarbosilane (PCS), manufactured by Nippon Carbon, supplied by Mitsui Plastics. The carbon fabric was cut into rectangular pieces, ca. 12 cm × 5 cm. 14 layers of these were stacked-up to provide the fibre preform ca. 4 mm thickness. A 50 wt.% PCS-hexane solution was used for the infiltration. The stacked preform was placed between two sheets of PTFE film, through which connector plates and tubes were linked to allow the PCS solution to flow through the reinforcement. The assembly was sealed in a similar manner to a vacuum bag. Under a vacuum of 0.7 atm, the PCS solution was allowed to infiltrate the fibre preform for 0.5 h and then left to soak for 1 Hr under atmospheric pressure. After drying in air with a low pressure applied to the surface, the green preform was cured in air. Curing for 1 h at 200 °C was carried out at a heating/cooling rate of 100 °C h^{-1}. Curing was carried out to prevent foaming of the composite on subsequent pyrolysis to convert the PCS polymer to ceramic. The details of the selection of the cure and pyrolysis conditions are reported elsewhere [16]. Pyrolysis was carried out at 1200 °C in vacuum. Four fibre preforms were prepared so that one underwent the infiltration, cure and pyrolysis cycle twice—referred to as having two infiltration cycles.

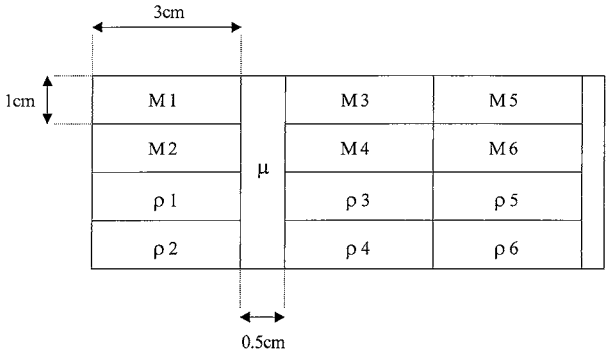

Figure 1 Plan of composite sections for characterization. M = mechanical test, ρ = density, μ = microscopy.

The second, third and fourth preforms received four, six and eight infiltration cycles respectively. The fibre volume fraction was ca. 45% in the final composite after 8 infiltration cycles. The four C/SiC-based CMCs produced were cut using a diamond wafering blade to provide samples for microscopy (μ), density measurement (ρ) and mechanical testing (M) as illustrated in Fig. 1.

2.2. Microscopy

For microscopy, samples were impregnated in a low viscosity epoxy resin under vacuum and the resin left to set. These were then polished to a 0.3 μm alumina finish. Microstructural analysis was carried out by light microscopy using an Olympus BH2 microscope, and scanning electron microscopy (SEM) using a Philips SEM505 operating at 20 KV.

2.3. Density measurement

The bulk densities of the composites were measured by the Archimedean method in water based on an ASTM standard test (C20-92) [17], from which the interrelated fractional open porosity can be calculated. The dry weight, D, was first measured in air. The sample was then soaked in water for 12 hrs after which the weight of the sample suspended in water, S, was determined. After this, the sample was lightly blotted with a damp cloth to remove surface water drops and weighed in air for the saturated sample weight, W. The sample exterior volume, V, was calculated from Equation 1.

$$V = (W - S)/\rho_o \tag{1}$$

The bulk density, B, was calculated from Equation 2.

$$B = D/V \tag{2}$$

where ρ_o is the density of water assumed to be 1 g cm^{-3} at room temperature.

From Equation 3, the volume of open pores, O, was obtained (by assuming that the density of water is 1 g cm^{-3}). The fraction of the volume of open pores was then expressed as a percentage of the exterior volume.

$$O = W - D \tag{3}$$

Five density measurements, using 5 sectioned pieces, were made for each of the CMCs except for the two times-infiltrated composite with which two measurements were made as delamination easily occurred on cutting.

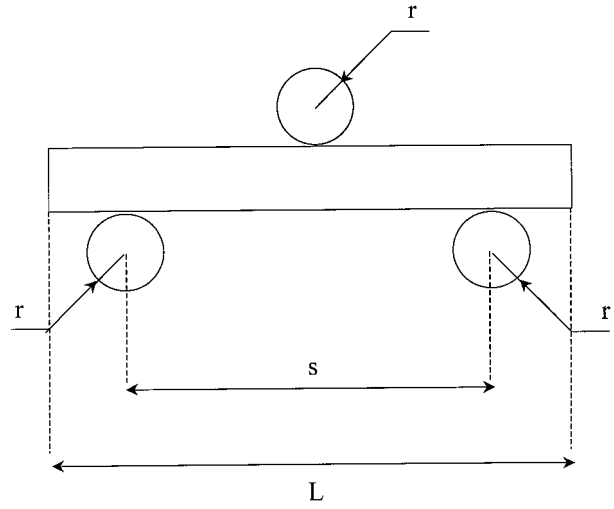

Figure 2 Three-point bend test jig.

2.4. Mechanical testing

Due to the relatively small size of the composites manufactured in this study, the interlaminar shear strength (ILSS) was measured using the short span three-point bend test. The ILSS is predominantly determined by the strength of the matrix and that of the interface. It is, therefore, important in studying the development of the matrix with the re-infiltration cycles. The tests were carried out on an Instron 4301 Universal testing machine at room temperature and were based on the European Prestandard (ENV 658-5) for ceramic composites [18]. The sample was set up in the test jig as shown schematically in Fig. 2. The test sample of length, L, width, b, and thickness, h, lies perpendicular on two steel support rollers which are capable of rolling outwards to allow relief of any frictional constraints. The load was applied via the central roller placed at the mid-point between and parallel to the two support rollers. The three identical rollers had a radius, r, of 3 mm, and the support span, s, was altered so that it was in the ratio within the range given by Equation 4.

$$s = 5h \pm 1 \tag{4}$$

This ratio has been reported to be a rough working rule for which shear failure will occur [19]. A crosshead speed of 0.5 mm min^{-1} was used. The shear failure force, F, was recorded and the interlaminar shear strength, τ, was calculated using Equation 5 [18].

$$\tau = 3F/4bh \tag{5}$$

Some of the samples, however, particularly the six and eight times infiltrated composites, appeared to fail in a tensile or mixed tensile/shear mode rather than the assumed plain shear mode. In this case, a shear failure stress was calculated if shear failure across the mid-plane (along the sample length) between the plies was observed to have occurred before tensile fracture through the thickness of the sample from the surface

TABLE I The changes in bulk density and open porosity with the number of infiltrations of samples taken from the C/SiC-based composites

Sample		Bulk density (g cm^{-3})		Open porosity (%)	
			Average		Average
X2 inf.	$\rho1$	0.90	0.82	53.18	56.3
	(ρ^3–ρ^4)	0.76	±0.07	59.36	±3.1
X4 inf.	$\rho1$	1.38	1.32 ±0.06	31.56	35.0 ±2.5
	$\rho2$	1.36		32.63	
	$\rho3$	1.33		36.04	
	$\rho4$	1.30		36.39	
	$\rho5$	1.21		38.14	
X6 inf.	$\rho1$	1.54	2.3 ±0.2	25.80	25.2 ±1.0
	$\rho2$	1.58		23.73	
	$\rho3$	1.52		26.18	
	$\rho5$	1.57		24.21	
	$\rho6$	1.53		26.01	
X8 inf.	$\rho1$	1.61	1.64 ±0.04	24.75	23.3 ±2.2
	$\rho2$	1.70		20.35	
	$\rho3$	1.60		25.36	
	$\rho4$	1.70		21.09	
	$\rho5$	1.61		25.34	

opposite the load point. If tensile failure was dominant, the flexural strength, σ, was calculated instead using Equation 6, where F is the recorded failure force, b, h and s are as described above.

$$\sigma = 3Fs/2bh^2 \quad (6)$$

In this case, even if tensile failure occurred before shear, a value of the ILSS was also calculated from the failure force to generate an estimate of the lower limit in the interlaminar shear strength.

Five measurements for the ILSS were made with the exception of the two times-infiltrated composites for which one result was obtained due to prior delamination of the sample.

3. Results and discussion

3.1. Density measurements

Shown in Table I are the bulk densities of samples sectioned from various parts of the composite for each of the composite. Also shown is the amount of open porosity. For each of the composites, the variations between the density values and the inter-related open porosity values can be attributed to a variability in the infiltration process and to sectioning, where some damage and loss of material occurred. This was a particular problem for the composites obtained with less than four infiltration cycles. A general trend can, however, be seen from these results, in that the bulk density tends to be higher in the samples taken from the outer edge regions ($\rho1$, $\rho2$, $\rho4$) than those taken from the central region ($\rho3$, $\rho5$) of the composite by up to around 6%. The average bulk density and open porosity of the composite produced according to the number of infiltration cycles are shown in Figs 3 and 4, respectively. These graphs show a gradual decrease in the infiltration efficiency with the number of infiltration cycles. After six infiltration cycles, the bulk density and the corresponding open porosity tends to a plateau, when after eight infiltration cycles,

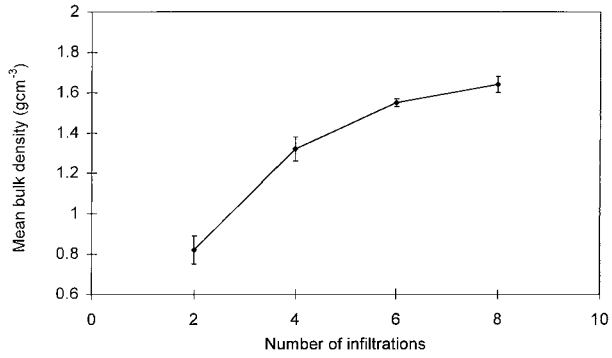

Figure 3 The change in the mean bulk density of the C/SiC-based composite with the number of infiltration cycles.

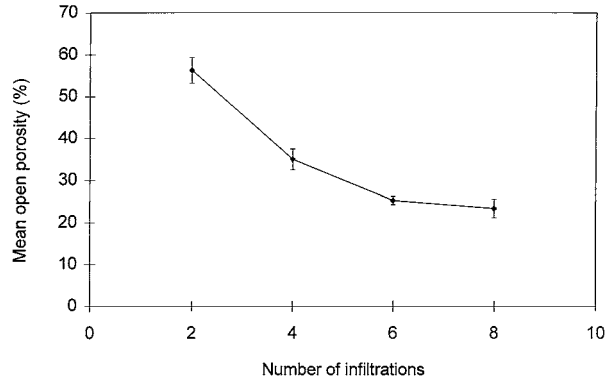

Figure 4 The change in the mean open porosity of the C/SiC-based composite with the number of infiltration cycles.

the average bulk density achieves 1.64 g cm^{-3} which represents an average open porosity of 23.4%. This is about 71% of the theoretical density (2.3 g cm^{-3}). The theoretical density being derived from the rule of mixture based on the density of the PCS-derived SiC-based ceramic matrix (2.8 g cm^{-3}) [20, 21], density of the carbon fibre fabric (1.76 g cm^{-3}), and the volume fraction of fibre (45%). The trend observed in this increase in density and hence decrease in open porosity suggests that after eight infiltration cycles, any further infiltration is unlikely to increase the density significantly as the amount of available open porosity and infiltration efficiency decreases.

3.2. Microscopy

After only two infiltration cycles, the resultant C/SiC-based composite is highly porous, with large voids particularly between the woven layers which can be seen in the optical microscope (Fig. 5). Segmentation of the fibre bundles can be seen in this optical view of the composite cross section. This is due to a relatively higher coefficient of thermal expansion of the carbon fibre transverse to the fibre axis, which creates transverse cracks as the matrix shrinkage is restrained parallel to the fibres, on cooling down from the pyrolysis temperature. On closer examination by SEM, the matrix distribution within the fibre bundles can be seen (Fig. 6). Only partial infiltration can be seen, leaving porous regions between the fibres, which may also be a result of the shrinkage cracks produced due to the volume contraction which occurs as the PCS polymer

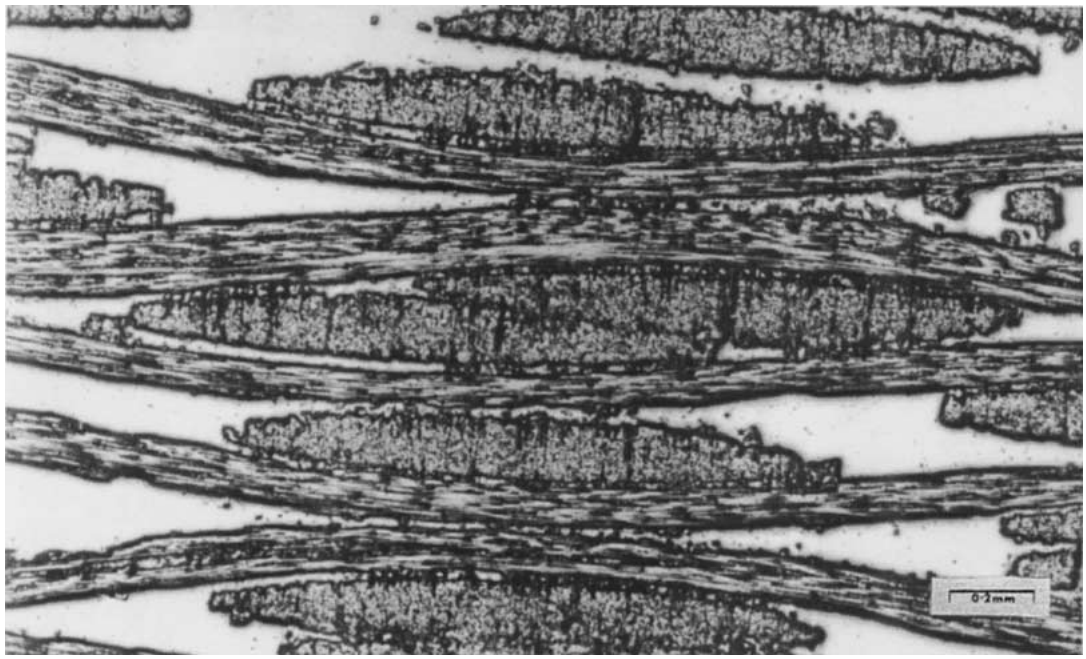

Figure 5 Optical micrograph of a cross-section of the C/SiC-based composite after 2 infiltration cycles.

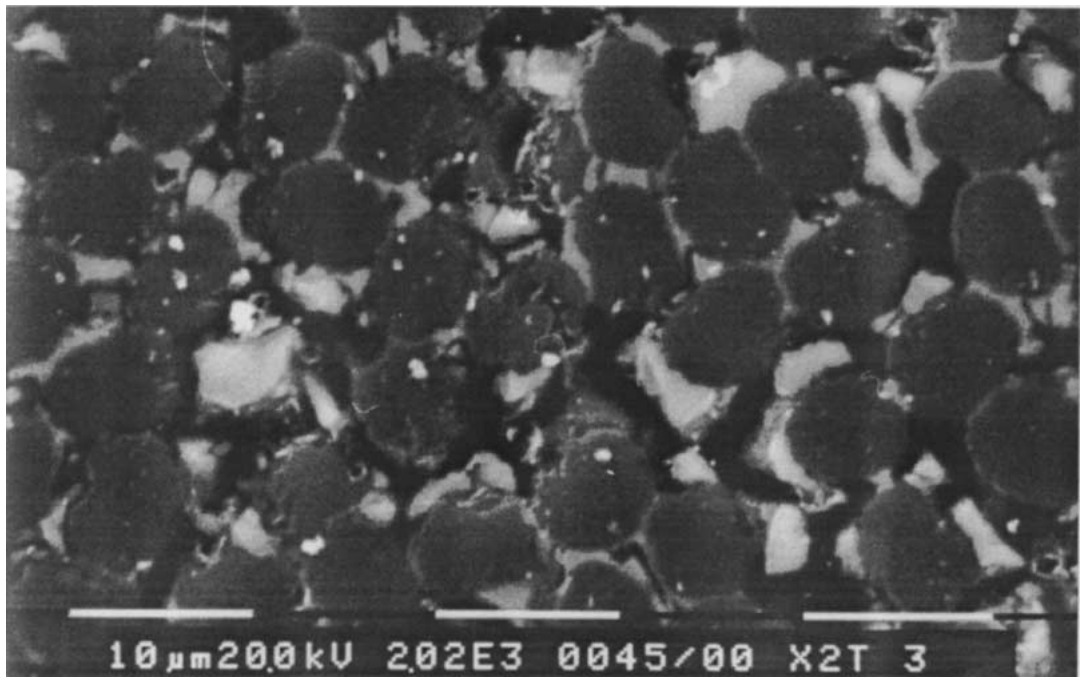

Figure 6 SEM micrograph of a cross-section of the C/SiC-based composite after 2 infiltration cycles.

undergoes pyrolytic conversion to ceramic. The low amount of matrix deposited may be expected since the ceramic yield obtained under these pyrolysis conditions was found to be about 76 wt.% [20]. The volume contraction was also found to be high (56%) [20], which may be the reason for some of the voids resulting from the polymer to ceramic conversion in these composites.

After four infiltrations, the PCS-derived SiC-based matrix fills up more of the inter-fibre voids with irregular porous regions remaining. The SiC-based matrix appears to bond well to the carbon fibres (Fig. 7). After the sixth re-infiltration cycle, there is a further improvement in the infiltration of the PCS into the voids between the fibre bundles (inter-fibre voids) and between the carbon fabric layers (inter-layer voids) (Fig. 8). As with all of these SiC-based composites, the core is generally more porous than the outer surface regions of the composite, suggesting that the infiltration has been most effective in the outer surface regions. The relatively dense outer regions would make the following infiltration into the central region of the composite less efficient. This microstructure variation is consistent with the density results found, where the density tended to be higher in the samples taken from the outer edge regions than those taken from the central region of the composite.

After the eighth infiltration cycle, a relatively dense composite can be seen in the optical micrograph of Fig. 9 which relates to the increase in density shown

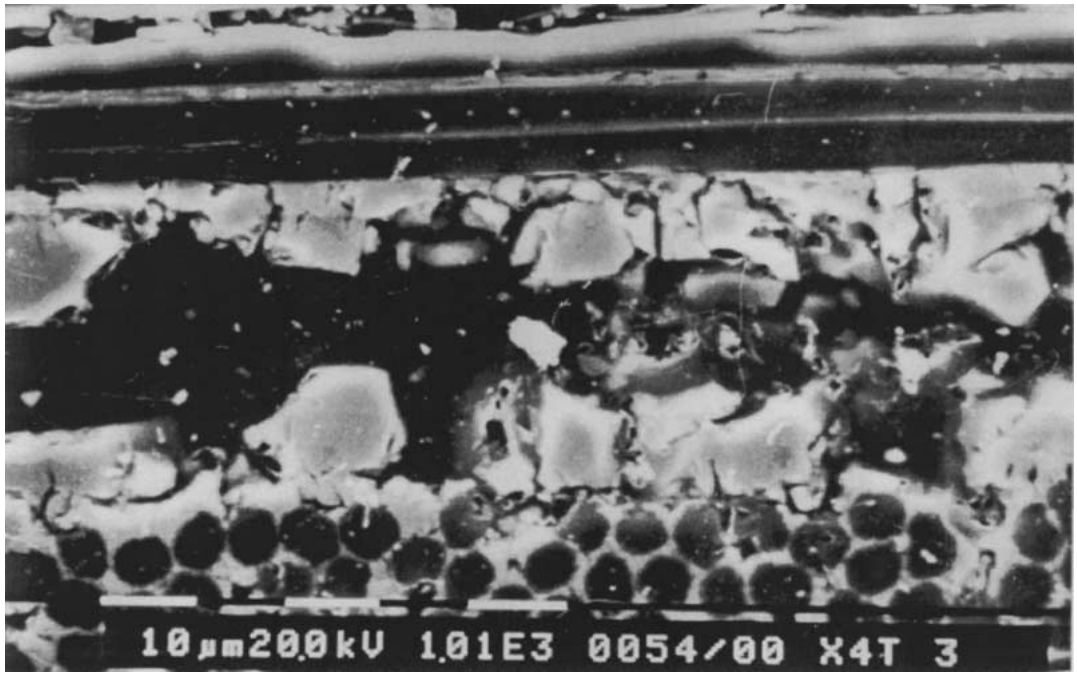

Figure 7 SEM micrograph of a cross-section of the C/SiC-based composite after 4 infiltration cycles.

Figure 8 Optical micrograph of a cross-section of the C/SiC-based composite after 6 infiltration cycles.

in Fig. 3. Transverse cracking of the matrix caused by cooling from the processing temperature can be seen in Fig. 9. A SEM micrograph of the local area (Fig. 10) shows relatively dense matrix distribution in the pores between the fibres within the fibre bundles, i.e. the inter-fibre voids, which is deposited before the larger diameter inter-layer voids. Some of these inter-layer voids can still be seen. Shrinkage cracks in the surrounding matrix can be seen. Some of these cracks may have already been created on drying of the composite after infiltration, as the solvent carrier evaporates. An increase in the bulk density and the corresponding decrease in the open porosity were found to tend to a plateau after eight infiltration cycles. Thus, it appears that the residual pores, particularly the closed pores in the eight times infiltrated composite may not be eliminated by any further re-infiltrations as the amount of available open porosity and infiltration efficiency decreases.

3.3. Mechanical testing

Results of the room temperature interlaminar shear strength (ILSS) of the composites, determined by the short-span three-point bend test, are given in Table II. The density changes are also shown to relate the changes in the mechanical property with the density of the composite. The mean ILSS and standard deviation from the set of results for each composite are shown

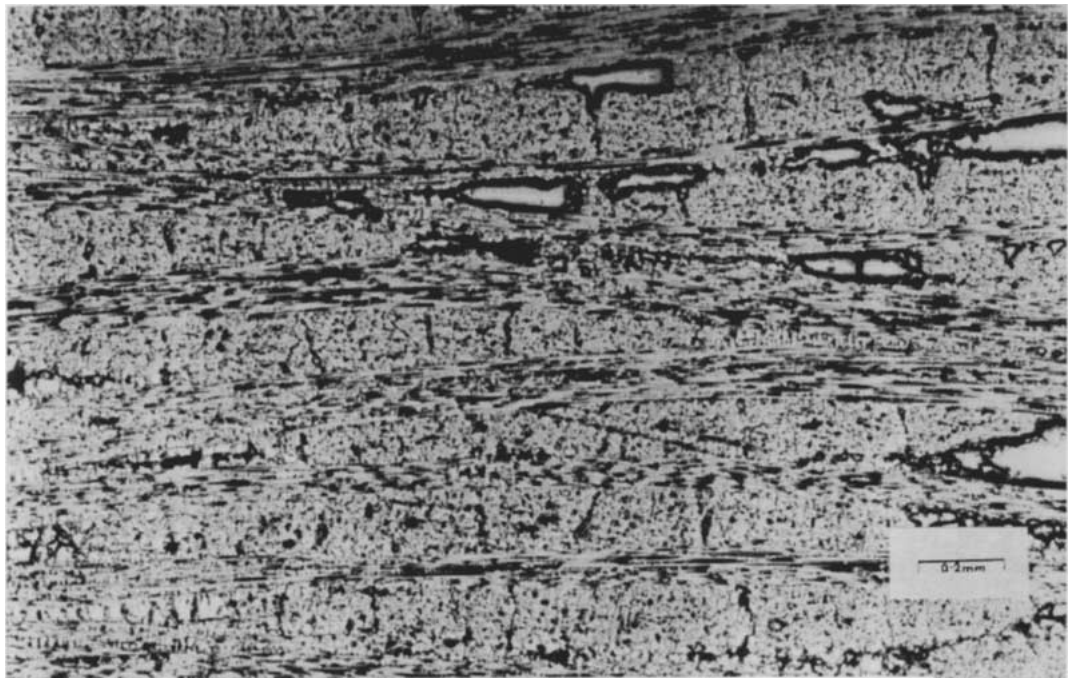

Figure 9 Optical micrograph of a cross-section of the C/SiC-based composite after 8 infiltration cycles.

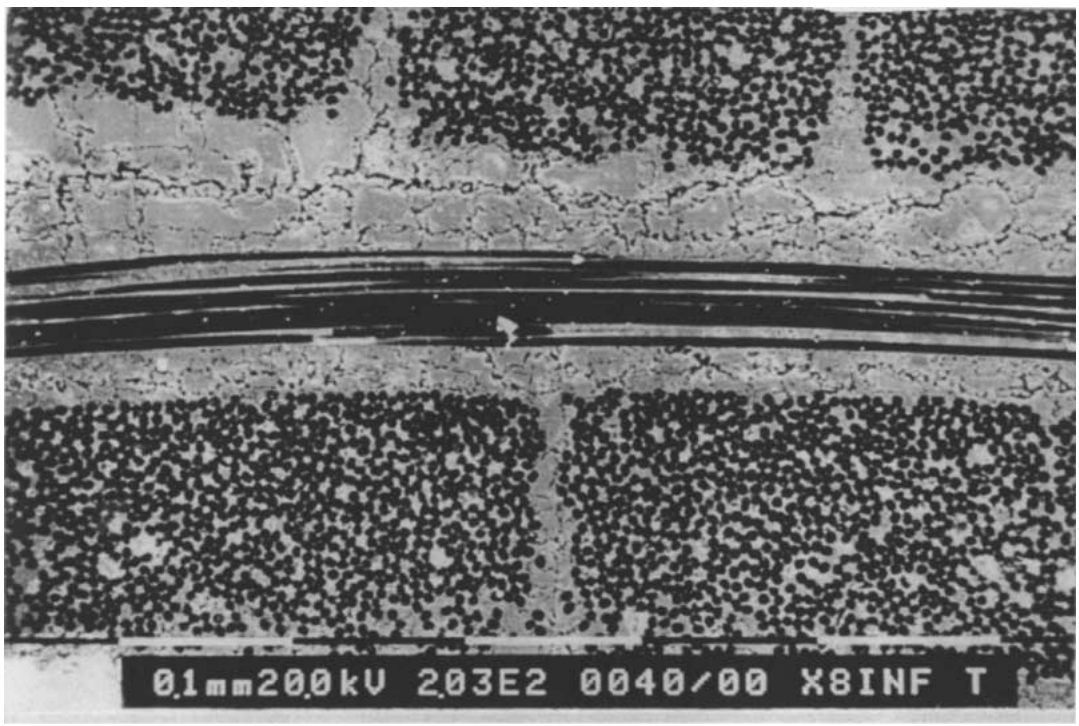

Figure 10 SEM micrograph of a cross-section of the C/SiC-based composite after 8 infiltration cycles.

graphically in Fig. 11. For some of the six times infiltrated samples and all of the eight times infiltrated samples, tensile failure was observed. This change in failure mode are discussed below. A mean flexural strength and standard deviation were obtained from these sample and the results (Table II), plotted in Fig. 12. For the eight times-infiltrated composite samples, interlaminar shear stress values, below their ultimate value, were also calculated using the tensile failure force, and an average value shown in Fig. 11. Typical load-displacement curves of these C/SiC-based composites in the three-point bend test are shown in Fig. 13a–d. Figs 14 and 15 are the photographs of a sample of the two and eight-times infiltrated composite after the three-point bend test.

The low volume of PCS-derived SiC-based matrix together with low adhesion between fibre and matrix found in the two times-infiltrated composite leads to a low interlaminar shear strength with gradual shear failure (Fig. 13a). Shear failure normally occured by delamination in the mid-plane of the sample parallel to the carbon fabric layer plane where the maximum shear stresses act, as shown in Fig. 14. After four infiltration cycles, shear failure occurred but at a higher

TABLE II Variation of the interlaminar shear strength (ILSS) or flexural strength (f) with the number of infiltrations of samples taken form the C/SiC-based composites

Sample		τ(Mpa)		σ(Mpa)	
			Average		Average
X2 inf.	M1	0.4	0.4		
X4 inf.	M1	0.81	0.9 ±0.3		
	M2	0.81			
	M3	1.33			
	M4	1.11			
	M5	0.60			
X6 inf.	M1	2.04	2.3 ±0.2		
	M2	2.97			
	M3	1.86			
	M5			11.60	11.9
	M6			12.13	±0.3
X8 inf.	M1	3.50	3.9 ±0.1	34.50	37.0 ±3.3
	M2	3.59		34.25	
	M3	4.28		41.98	
	M4	3.61		34.43	
	M5	4.29		39.96	

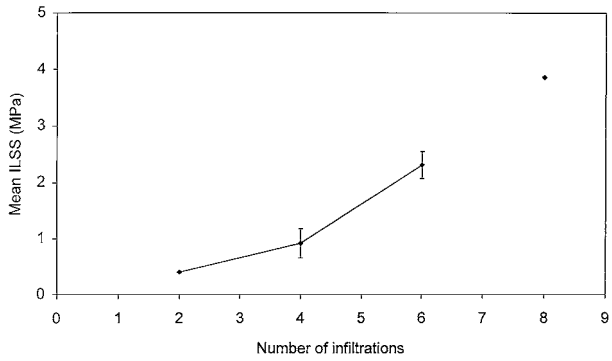

Figure 11 The change in the mean interlaminar shear strength (τ) of the C/SiC-based composite with the number of infiltration cycles.

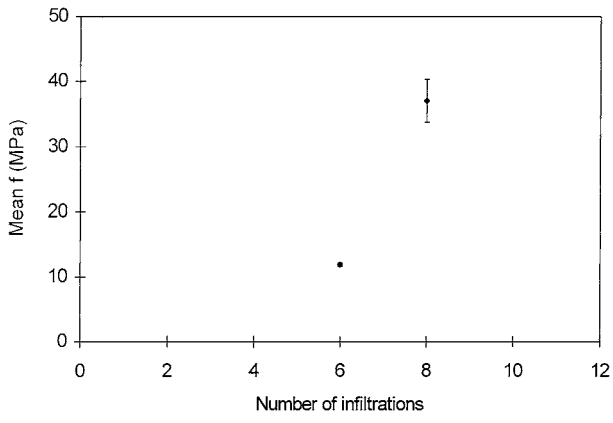

Figure 12 The change in the mean flexural strength (σ) of the C/SiC-based composite with the number of infiltrations.

shear failure stress (Table II) as the composite density increased. Samples M3 and M4 of this four times-infiltrated composite had a smaller thickness than other test specimens, being about half that of the original composite thickness due to separation on cutting. These two samples (M3, M4) had densities which were higher than the average density of the other samples, due to the porosity being higher in the middle of the sample. A typical load-displacement trace in the three-point bend test

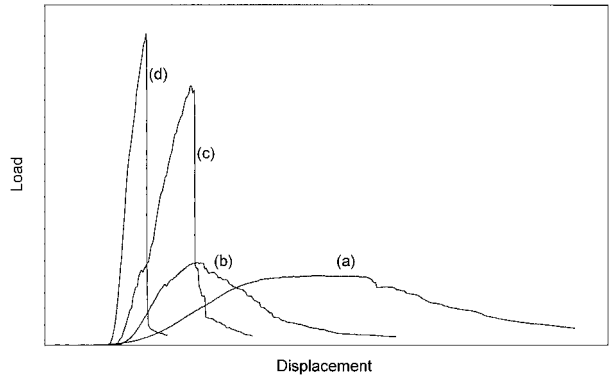

Figure 13 Typical load-displacement curves in the three-point bend test at room temperature of the C/SiC-based composite produced by (a) 2 ; (b) 4 ; (c) 6 and (d) 8 infiltration cycles.

of the four times-infiltrated composite seen in Fig. 13b show a gradual failure similar to that found for the composite produced after two infiltration cycles. Some fibre pull-out was observed using SEM and this will contribute to the step-drop in the load displacement curve.

After six infiltration cycles, higher interlaminar shear strengths were obtained as the density gradually increased (Table II). Although a higher interlaminar shear strength was found, the six times infiltrated sample showed a more catastrophic failure, where a more sudden continuous drop in the load can be seen in the three-point bend trace (Fig. 13c). A mixed failure mode was observed for samples M5 and M6 where tensile failure appeared to have started under the mid-load point on the side of the support roller (point of maximum tensile stress) before any shear delamination. In this case, a flexural strength was calculated (Table II). This typical brittle-like failure is due to a stronger fibre-matrix bond which was seen under the SEM (not illustrated). This may be expected as the SiC-based matrix obtained after the first infiltration cycle would effectively have experienced sintering for six hours at 1200 °C after the sixth infiltration cycle.

After eight infiltration cycles, a crack path perpendicular to the plane of the sample began at the tensile surface on the side of the support rollers for all of the samples. There was no apparent delamination (Fig. 15) indicating a plain tensile failure mode when compared to the mixed failure mode found for the composite formed with six infiltration cycles where the tensile through-thickness crack was more tortuous. An instantaneous drop in the load following the maximum was typical of the load-displacement trace for this eight-times infiltrated composite (Fig. 13d). The higher amount of matrix formed and degree of fibre-matrix bonding should be the main contributing factor to the higher interlaminar strength, with little sliding giving a brittle fracture. Reaction between the carbon fibres and the oxide-containing SiC-based matrix on pyrolysis is also a possible cause in the embrittlement of the composite, leading to degradation of the carbon fibre itself.

The transition in failure mode from shear to tensile may be explained by the increase in the interlaminar shear strength of the composite with the number of infiltration cycles. The ratio of tensile stress to shear stress

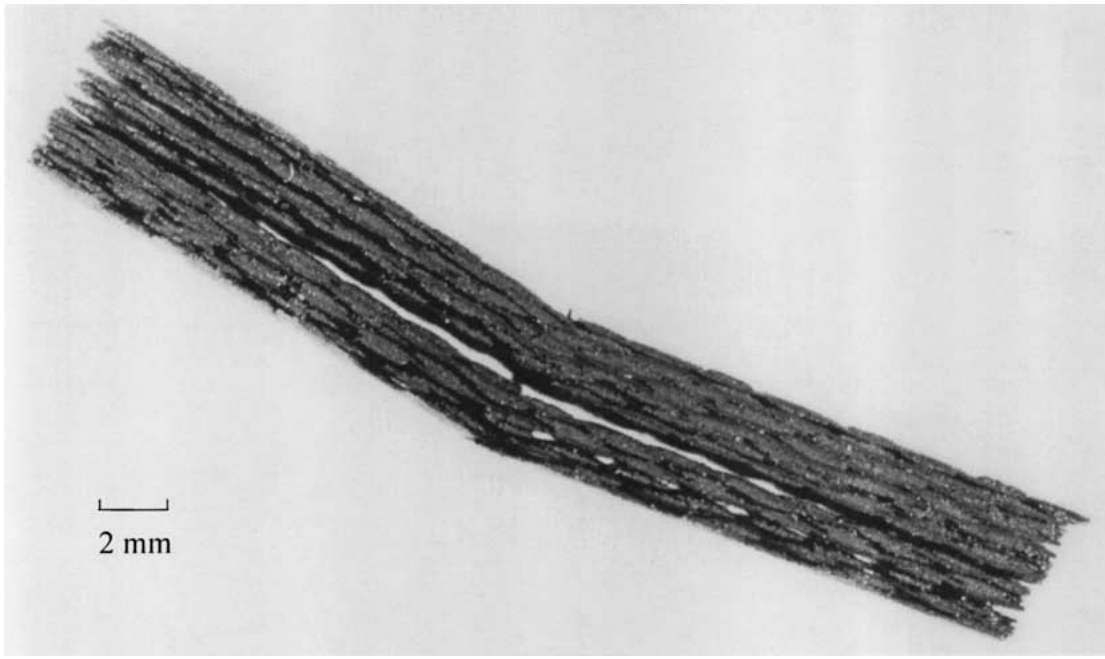

Figure 14 Photographic view of the C/SiC-based composite sample after the three-point bend test at room temperature (2 infiltration cycles).

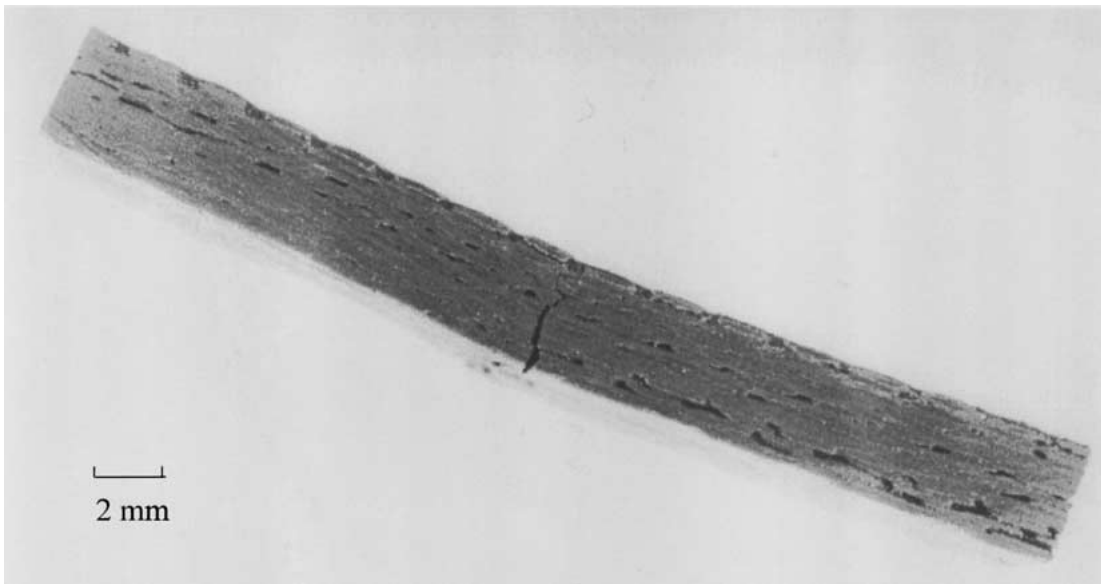

Figure 15 Photographic view of the C/SiC-based composite sample after the three-point bend test at room temperature (8 infiltration cycles).

($\sigma : \tau$) is proportional to the ratio of the 3-point test support span to sample thickness ($s : h$) [19]. As the load is increased, failure occurs when one of these reaches its critical value. The failure mechanism, thus, depends on the relative values these ratios. To an approximation, shear failure will occur if $s/h < (\sigma/\tau)$ and tensile failure if $s/h > (\sigma/\tau)$ [19]. Thus, as the interlaminar shear strength, τ, increases with the number of infiltration cycles, a tensile failure may be favoured rather than the assumed shear failure estimated from the rough working rule given in Equation 4. There was no clear trend between the interlaminar shear strength and the region of the composite from which the test samples were cut, although samples from the outer surface region tended to show a higher value than the samples taken from the central region of the composite. This is consistent with the fact that samples taken from the outer surface regions of the composite were generally denser than the more porous central regions of the composite. Since the centre of the composite tended to be more porous and the maximum shear stress occurs on mid-plane along this central region, shear delamination at a low shear strength can be expected particularly for the composites with less than 6 re-infiltrations. The non-uniform deposition of matrix around the fibres with varying distribution of void size and shape, microcracked matrix caused by the composite processing before the mechanical test would contribute to the varying local stress concentrations and thus the variations in results. The problem of an additional tensile failure mode rather than the assumed plain shear failure is possible in the short beam three-point bend test but can be difficult to distinguish. The lower limit of the interlaminar shear strength obtained in this work for the eight times infiltrated C/SiC-based composite was of 3.9 MPa which is in the range (1.5–15 MPa) reported by Thielicke and

Soltesz [22] for a 0/90° laminated C/C composite tested in a similar three-point bend test. There were no reported ILSS values for similarly PCS-derived composites in the literature. ILSS values between 25–30 MPa has been reported for C/SiC composites produced by the liquid silicon route [23] and by CVI [24]. The lower ILSS values of the composites produced in this study is mainly caused by retained porosity. This PCS infiltration process is, however, less costly and time consuming than the CVI and liquid silicon routes.

4. Conclusions

There are essentially two types of voids in the composite, i.e., the larger interlayer voids and the smaller inter-fibre voids. This resulted in a non-uniform distribution of the matrix on infiltration, where the smaller pores were filled first. There was dense deposition of the matrix on the outer surface, sealing off the core of the composite, which hindered successive infiltrations. After six infiltration cycles, the density increase tends towards a plateau. The average density of 1.64 g cm^{-3} was achieved after eight infiltration cycles, which represents an average open porosity of 23.4%. The trend indicated that further infiltrations will not increase the density significantly. The density results are consistent with the observed composite cross sections which showed a more porous central region compared to the denser outer surface. The denser parts of the composite also corresponded to higher mechanical properties. As the density of the composite increased with the number of infiltrations, so did the interlaminar shear strength, which is a measure of the degree of bonding between the fibre and matrix. However, the failure became more brittle with further infiltration cycles. Samples of the composite obtained after two, four and six infiltration cycles failed in a predominantly shear mode by delamination between the layers. On the other hand, the eight times infiltrated composite showed a plain brittle tensile failure with no apparent delamination. This was accompanied by a gradual to catastrophic failure transition due to an increase in the amount of matrix and the degree of bonding with the fibres. The greater amount of matrix increased the interlaminar shear strength thus making tensile failure more probable. This PCS-derived SiC-based matrix can react with the carbon fibres as it contains oxide phases and thus may have occurred to a great extent as the number of pyrolysis cycles increased. Hence degradation of the fibres as well as the matrix may occur.

References

1. J. A. CORNIE, Y. M. CHIANG, D. R. UHLMANN, A. MORTENSEN and J. M. COLLINS, *Amer. Ceram. Soc. Bull.* **65** (1986) 293.
2. C. GRENET, L. PLUNKETT, J. B. YEYRET and E. BULLOCK, *Ceram. Trans.* **58** (1995) 125.
3. K. NAKANO, A. KAMIYA, M. IWATA and K. OSHIMA, "Developments in the Science and Technology of Composite Materials," 3rd ed. (ECCM, Bordeaux, France, 1989) p. 381.
4. R. KOCHENDORFER, in Proc. ICCM, 1991, p. 23-F2.
5. C. V. BURKLAND and J.-M. YANG, *SAMPE Journal* **25** (1989) 29.
6. D. HEIMANN, J. BILL, F. ALDINGER, P. SCHANZ, F. H. GERN, W. KRENKEL and R. KOCHENDORFER, *Z. Flugwiss. Weltraumforsch.* **19** (1995) 180.
7. F. I. HURWITZ, P. J. HEIMANN, J. Z. GYEKENYESI, J. MASNOVE and X. Y. BU, in 15th Annual Conference on Composites and Advanced Ceramics, 1991, p. 1.
8. H. O. DAVIS and D. R. PETRAK, *J. Nucl. Mater.* **219** (1995) 26.
9. R. P. BOISVERT and R. J. DIEFENDORF, *Ceram. Eng. Sci. Proc.* **9** (1988) 873.
10. T. TANAKA, N. TAMARI, I. KONDOH and M. IWASA, *J. Ceram. Soc. Jpn. Int. Ed.* **103** (1995) 1.
11. S. RICCITIELLO and M. K. MARSHALL, *J. Adv. Mater.* **25** (1994) 22.
12. *Advanced Materials* **16** (1994) 1.
13. B. SU, F. R. LIU, X. J. LIU and X. Y. WANG, in ICCM/9 Metal Matrix Composites : Proc. Conf., 1993, Vol. 1, p. 464.
14. S. P. APPLEYARD, X. X. JIANG and B. RAND, *Key Engineering Materials* **127–131** (1997) 263.
15. W. D. VOGEL and U. SPELZ, *Ceram. Trans.* **51** (1995) 255.
16. H. Q. LY, R. TAYLOR, R. J. DAY and F. HEATLEY, *J. Mater. Sci.* **36** (2001) 4045.
17. ASTM standards C20-92, 1992.
18. "Advanced Technical Ceramics—Mechanical Properties of Ceramic Composites at Room Temperature. Part 5 : Determination of Shear Strength by Short Span Bend Test (three-point)," European Prestandard, ENV 658-5, 1993.
19. R. W. DAVIDGE and J. J. R. DAVIES, *Int. J. High Technology Ceramics* **4** (1988) 341.
20. H. Q. LY, Ph.D. Thesis, 1997.
21. M. MONTHIOUX and O. DELVERDIER, *J. Eur. Ceram. Soc.* **16** (1996) 721.
22. B. THIELIKE and U. SOLTESZ, in Proc. ECCM. Conf. Testing & Standardisation, 1992, p. 287.
23. P. SCHANZ and W. KRENKEL, in 6th EACM-CMC1., 1993, p. 715.
24. A. LACOMBE and J. M. ROUGES, in Space Programs and Technologies Conference, 1990, p. 1.

Received 14 April
and accepted 14 December 1999